CHAPTER 4

ERROR COMPENSATION AND UNCERTAINTY ANALYSIS IN DIRECT INTERFACING E-NOSE

4.0. Introduction

As mentioned in chapter 1 and chapter 3, direct interfacing circuit (DIC) based methods are gaining popularity for sensor response measurement due to their design simplicity, low power consumption, less space requirement and cost-effectiveness. However, DIC based model [4, 6, 26] that can minimize the errors in the measurement system for real-time applications with higher reliability is an essential requirement [7, 20]. Although many research efforts have focused on the various application of DICs such as resistance [7, 17, 20, 21], capacitance [11, 15, 22, 24], inductance [16] and analog voltage [3, 18, 28], the possible framework that can minimize the error in the measurement is less exploited.

In chapter 3, design, implementation and analysis of DIC based multisensory E-Nose framework was discussed. The capability to efficiently classify different gases is validated through a FFBP ANN implemented in μC. These results shows that it is possible without the need of an ADC to effectively measure the counter value as a feature of analog voltage by the MCU and also the measured counter values can be used to model pattern recognition tools. However, the DIC model poses nonlinearity error and fails to accurately interpret the measured voltage in terms of count value. This affects the accuracy of the measured responses from the sensor array by the E-Nose system, and can lead to inaccurate interpretation. Therefore, one of the objectives of this chapter is to incorporate an error compensation algorithm in the μC that will instantly reduce the nonlinearity error during measurement.

Another objective of this chapter is detailed analysis of all the uncertainty sources inherent in a DIC-based E-Nose. The uncertainty caused by the sensor circuit and DIC parameters in measurement of output responses from a MOS gas sensor array is also estimated. In deriving such a setting, uncertainty principle is utilized to estimate ranges of the uncertainty of each parameter that causes a deviation in measurement from the true value. The efficiency of the E-Nose relies both on the DIC parameters and sensor parameters such as gas concentration, exponent of power law etc and therefore the uncertainties associated with these parameters, their estimations and control are of prime importance to have better output responses. Experimental investigation demonstrates that DIC interfaced MOS gas sensor based E-Nose incorporates various sources of uncertainty.

4.1. Error Compensation

The minimization of nonlinearity (i.e., errors) in the DIC-based method not only relies on design parameter but also on the calibration techniques [20]. The extent of the nonlinearity indicates the reliability of design model for real-time implementation [19, 20]. Thus an appropriate model is direly needed to achieve the lowest possible value of this parameter. Reverter et. al in [20] adopted three such techniques in the context of accuracy and resolution of direct resistive sensor-to-µC interfaces that yielded an error of 0.01%. In the context of achieving suitable measurement setup, various approaches estimated the possible nonlinearity in the interfacing circuits. In [19] the authors estimated the DIC-interfacing error in capacitance measurement. Recently, Kokolanski et. al in [16] proposed a µC-based interface circuit for inductive sensors. The method resulted in nonlinearity up to 0.3% of the full-scale span with 10-bit resolution. A simple direct analog-to-µC interfacing method for measuring analog signal is demonstrated in [3]. The sensor analog voltage is effectively measured using two external resistances and a capacitor. Although it works similar to the measurement obtained using 12-bit ADC, the measured outputs deviate from that of an ideal one which introduces a significant level of nonlinearity. Despite potential benefit due to design simplicity, the research did not explore the use of efficient nonlinearity reduction strategy to enhance the viability of measurement.

Most of the aforementioned applications mainly focus on single sensor based DIC analysis with special emphasis on measurement procedure. However, DIC implementation for multi-sensor applications with an efficient calibration technique has not yet been explored. Recently, a method was developed for multi-sensor-DIC using MOS gas sensors in [9] and was shown to be useful in the multisensory environment. To further improve the nonlinearity and wider viability of the approach for measurement processes, it is essential to adopt more robust and reliable calibration strategy which motivated our study.

As mentioned in chapter 1, a linearized DIC-multi-sensor (LDIC-MS) is presented which integrates the interfacing of analog signals to µC design model [3] to measure the individual sensor responses and collected outputs are analyzed using data-driven model. In linearizing the measurement, calibration was performed using compensating model so that it behaves similarly to that of the successive approximation based inbuilt- µC ADC. The proposed LDIC-MS not only focus on the possible aspect of DIC in multi-

dimensional implementation but also evaluate the best compensating model using inter-cross validation technique over real-time data. The merit of the proposed approach is that it linearizes the output measures towards ideal and is more suitable for sensor applications with higher reliability.

The main contribution of the proposed error compensation technique is summarized as:

1) It provides a potential solution to compensate nonlinearity in the measured output in an efficient way so as to accurately map the non-linear direct interfacing based ADC **(**nADC) to that of an ideal ADC.
2) Application of the best fit model for online error compensation using µC.
3) Implementation of the proposed framework in a multisensory environment and improved level of analysis ensuring higher reliability.

The effectiveness of the LDIC-MS is examined considering an intelligent multi-sensor electronic nose which is used as an identification marker for gas classification, food quality assessment etc. [32, 33]. Although various data-driven models such as SVM, LDA etc. [33, 34] are popular for classification task, the presented work adopted a three-layer feed forward back propagation neural network model due to its popularity in digital systems and it poses high flexibility, accuracy, better repeatability and testability, lower adaption to noise, and higher compatibility [10]. Study and compensation of drift, discreteness, and disturbances have been conducted in [32, 33] however the proposed work focuses on error and nonlinearity compensation of the DIC considering that the short time drift of the sensors is very low. Moreover, in this work the experiments were conducted under constant ambient conditions without any environmental disturbances. An attempt is made in this work to show that the developed LDIC-MS is efficacious and more reliable. It is pertinent to mention herein that the MOS gas sensors require two separate power sources one for the sensor heater and the other for the sensor itself. The sensor heater voltages for each of the sensors are supplied from a separate power supply, so the rest of the MOS sensor works similar to any resistive sensor. Therefore the proposed work can be an opportunity for low power embedded systems where multiple sensor outputs are to be measured accurately. Moreover, based on the requirement the measured responses can be used to perform certain tasks.

4.1.1.Non-linear direct interfacing based ADC (nADC)

As mentioned in chapter 3, Fig. 4.1 shows the DIC implemented in the µC for measurement [3]. The sensor output voltage V_{in} is measured in terms of counter value implementing the following steps in the µC. The charging and discharging path of the DIC is- first the capacitor C is charged to V_{in} through R_2 by configuring port D_0 and D_1 as high impedance inputs and a counter value N_0 is initialized. We compare whether C is charged to a value higher than or equal to the input logic high V_{IH} of the µC or not. If the voltage across the capacitor is $\geq V_{IH}$ then the capacitor is discharged through the resistance R_1 by configuring D_0 as logic low V_{IL} digital output and the counter value is incremented. Otherwise, the capacitor is charged through R_1 by configuring D_0 as logic high digital output and counter value is decremented.

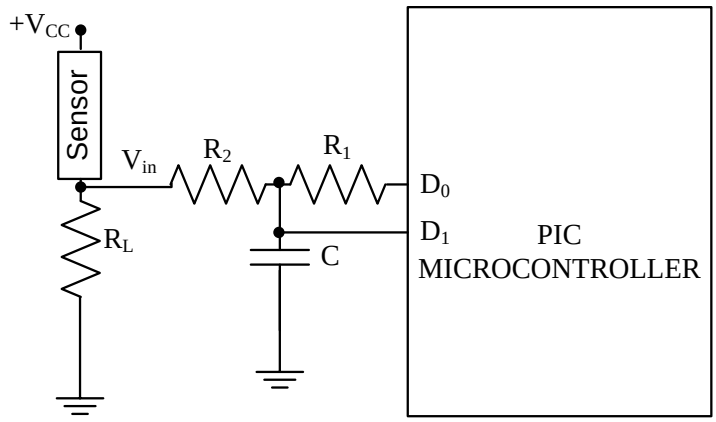

Fig. 4.1. Direct interfacing circuit.

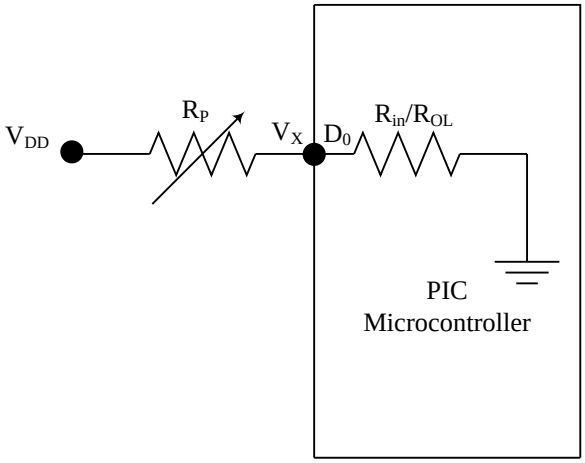

Fig. 4.2. Circuit diagram for measurement of R_{OL} .

The discharging time t_d and charging time t_c is proportional to V_{in} and $(V_{IH} - V_{in})$ respectively. Thus a counter value proportional to the analog voltage is considered as the measure of the analog voltage. During charging/discharging the input impedances of the I/O-pin of the µC when set high and low are ideally low and found as 112.12 Ω and 47.06 Ω respectively [20].

Fig. 4.2 illustrates the circuit used to measure R_{OL}. In doing so, I/O-pin D_0 is configured as output logic low and then an infinite loop is created in the code in order to execute it. V_X is measured and set at 0 V by tuning the potentiometer. R_{OL} is estimated by increasing the voltage across I/O-pin D_0 by tuning the potentiometer. Careful fine tuning of the potentiometer is required in order to ensure the exact position at which the voltage across V_X is equal to $V_{DD}/2$. The resistance of the potentiometer at that position is the value of R_{OL}, which is measured by a precision multimeter (Keithley 2110).

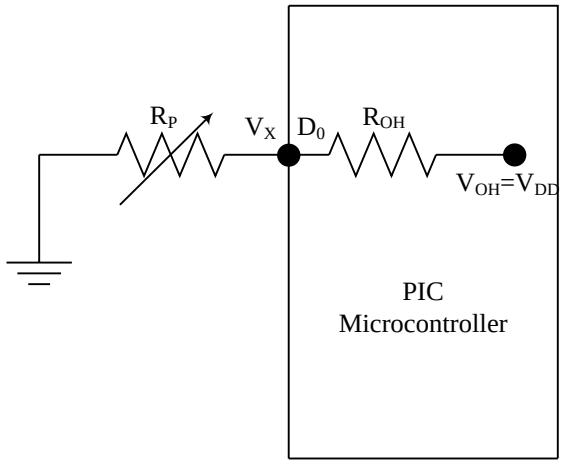

Fig. 4.3. Circuit diagram for measurement of R_{OH}.

Fig. 4.3 shows the circuit used to measure R_{OH}. The I/O-pin D_0 is configured as output logic high and the open circuit voltage is measured across it to ensure that $V_{OH} = V_{DD}$. In contrast to the measurement of R_{OL}, I/O-pin D_0 is reconfigured as output logic high and then an infinite loop is created in the code in order to execute it. V_X is measured and set at V_{DD} by tuning the potentiometer. R_{OL} is estimated by decreasing the voltage across I/O-pin D_0 by tuning the potentiometer. Careful fine tuning of the potentiometer is required in order to ensure the exact position at which the voltage across V_X is equal to $V_{DD}/2$. The resistance of the potentiometer at that position is the value of R_{OH}, which is measured by a precision multimeter.

To effectively measure the corresponding count value of V_{in}, we need to find out the starting counter value N_0 and the delay to be provided while up-counting (D_c) and down-counting (D_d). The value of N_0, D_C and D_D are computed using equation (4.1-4.5) [3] given by:

$$t_d = -\frac{1}{(1/C)((1/R_1)+(1/R_2))} \cdot \ln\{\frac{1}{R_2}(\frac{V_{IL}(R_1+R_2)}{(V_{in})} - R_1)\} \tag{4.1}$$

$$t_c = -\frac{1}{(1/C)((1/R_1)+(1/R_2))} \cdot \ln\{(\frac{V_H(R_1+R_2) - R_2V_{DD} - R_1(V_{in})}{R_2 \cdot (V_{in} - V_{DD})})\} \tag{4.2}$$

$$N_0 = \frac{t_{c,\max}}{t_{c,\max} + t_{d,\max}} \times 2^{12} \tag{4.3}$$

$$D_d = \frac{F_0 \cdot t_{d,\max}}{4 \cdot (2^{12} - N_0)} - 9 \tag{4.4}$$

$$D_c = \frac{F_0 \cdot t_{c,\max}}{4 \cdot N_0} - 9 \tag{4.5}$$

where, the maximum value of the charging and discharging time is found to be $t_{d,\max} = 8.5\text{ms}$ by setting $V_{in} = V_{DD}$ in (4.1) and $t_{c,\max} = 4.5\text{ ms}$ by setting $V_{in} = 0$ in (4.2) respectively. These values are determined by using known values of resistances, $R_1 = 3.1979\ \text{K}\Omega$ and $R_2 = 9.861\ \text{K}\Omega$ having 0.1% tolerance, capacitance $C = 2.255\ \mu\text{F}$ having 5% tolerance, $V_{IH} = 1.962\ \text{V}$ with a tolerance of 5%, $V_{IL} = 1.880\ \text{V}$ and supply voltage $V_{DD} = 4.65\ \text{V}$. The values of N_0, D_C and D_D are calculated using (4.3-4.5) and are found to be 1412 and 7 instruction cycles for both the cases. The frequency (F_0) of the crystal oscillator used is 20 MHz.

We divide the full span counter value in the range of 0 to 4095 to represent a 12-bit ADC using equation (4.3), while the inbuilt ADC of the PIC 18F45K22 is of 10-bit. Moreover, in order to maintain the speed resolution trade-off [20], we have chosen a capacitor $C = 2.255\ \mu\text{F}$, which fulfills the systems resolution. For the DIC the sampling time depends on V_{in} and the sampling rate is determined considering $V_{in} = V_{DD}$ where maximum discharging time $t_{d,\max}$ is required. Therefore, the sampling rate of the DIC used is found to be 117 Hz $(1/t_{d,\max})$. Whereas, in case of internal ADC of the PIC higher sampling rate up to 31 KHz can be achieved. Although, the nADC system is slow

compared to the ADC it does not limit our analysis in case of sensors response acquisition. Precise measurement and calculation of different parameters were done in order to minimize the uncertainty caused by the E-Nose system on the sensor responses.

The features for ANN classification has been extracted using (4.6):

$$\Delta V_{in,i} = V_{p,i} - V_{b,i} \tag{4.6}$$

where, $V_{p,i}$ and $V_{b,i}$ are the peak and baseline responses of the i^{th} sensor. Measurement of $V_{p,i}$ and $V_{b,i}$ are a slow process, compared to the fast varying signals, therefore the lower sampling rate of 117 Hz does not affect the accuracy of the system. This differential mode of feature extraction in the µC inherently cancels out the common noise present in the signals. Moreover in direct-interfacing mode it eliminates the effect of any offset voltage present in the signals. The DIC based analysis presented here can be achieved by using any microcontroller following the design guidelines presented in Chapter 3 and Chapter 4.

4.2. Error Compensation

The calibration characteristic of direct interface model shown in Fig. 4.1 is analyzed by applying analog voltage from 0-V_{DD} using a precision power supply (Agilent E361A). The characteristics of measured counter values with input analog voltage and the ideal characteristic are shown in Fig. 4.4.

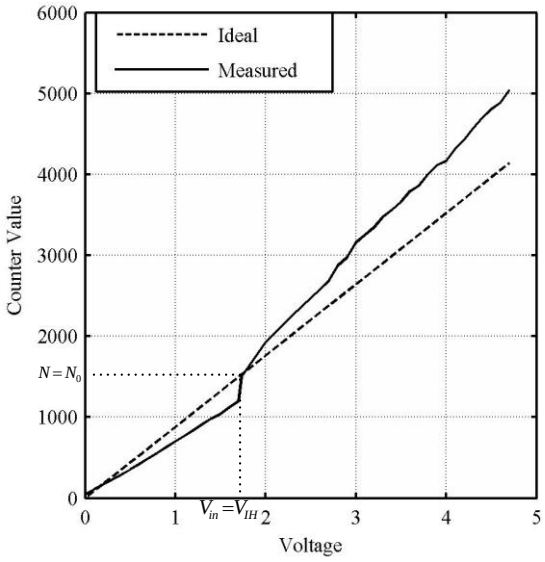

Fig. 4.4. Characteristics of Ideal ADC and nADC.

The plot shows that the maximum deviation of the measured value when $V_{in} < V_{IH}$ is found as 301 counter values while it is 833 counter values when $V_{in} \geq V_{IH}$. There are distinctly two different slopes of the measured values for the two cases- $V_{in} < V_{IH}$ and $V_{in} \geq V_{IH}$, with a transition voltage of $V_{in} = V_{IH}$.

We have made an attempt to linearize the characteristic using several error compensation techniques as shown in Table 4.1. It is observed that Power model of order 2 best fits the model in terms of root mean square error (RMSE) and the number of coefficients. Therefore we have used the Power-2 model which linearizes the output using a least square based approximation algorithm to fit the characteristic to a model equation. The model is then simulated in the PIC μC to calibrate the nonlinear measurements to linearize counter values.

We approximate the nADC counter data $\hat{X}[x_1, x_2, ..., x_n]$ for the range $V_{in} < V_{IH}$ (0-1.8 V) to a linear ideal data $\hat{Y}[y_1, y_2, ..., y_n]$ and similar approximation is made for the range $V_{in} \geq V_{IH}$ (1.9- V_{DD}). In this process, a best fit two-term model is obtained given by:

$$\hat{Y} = a \cdot X^{b} + c \tag{4.7}$$

where, the coefficients a, b and c are estimated by using least square model based on Levenberg-Marquardt (LM) iterative algorithm.

Table 4.1 Error Compensating Models.

Fit Function-Degree	Generalized Equation	SSE		RMSE		No of coefficients	Memory Consumption
		$V_{in} < V_{IH}$	$V_{in} \geq V_{IH}$	$V_{in} < V_{IH}$	$V_{in} \geq V_{IH}$		
Exponential-1	ae^{bX}	2.65×10^{5}	1.44×10^{5}	128.2	74.57	2	low
Exponential-2	$ae^{bX} + ce^{dX}$	365.6	1.49×10^{4}	5.11	24.92	4	high
Fourier-1	$a_0 + a_1\cos(Xw) + b_1\sin(Xw)$	571.8	1.37×10^{4}	6.391	23.93	4	high
Fourier-2	$a_0 + a_1\cos(XW) + b_1\sin(XW)$ $+a_2\cos(2XW) + b_2\sin(2XW)$	255.5	1.09×10^{4}	4.615	22.3	6	Very high
Gaussian-1	$a_1e^{(-((X-b_1)/c_1)^2)}$	4.19×10^{4}	1.41×10^{4}	57.25	23.77	3	high
Gaussian-2	$a_1e^{(-((X-b_1)/c_1)^2)} + a_2e^{(-((X-b_2)/c_2)^2)}$	9140	1.25×10^{4}	27.6	23.86	6	Very high
Power-1	aX^{b}	6321	4.07×10^{4}	19.88	39.6	2	low
Power-2	$aX^{b} + c$	**411.5**	1.43×10^{4}	**5.238**	**23.97**	**3**	**low**
Polinomial-1	$p_1X + p_2$	2761	2.40×10^{4}	13.14	30.38	2	low
Polinomial-2	$p_1X + p_2X + p_3$	571.8	1.48×10^{4}	6.174	24.35	3	high

The least square approximation fits a function $\hat{Y}(t,P)$ of an independent variable t with a vector of n parameters X to a set of n data points (t_i, X_i) by minimizing the sum of the weighted squares of the errors (or residuals) between the measured $X(t_i)$ and the curve fit function $\hat{Y}(t_i,P)$ [12]. This scalar valued goodness of fit measure is called chi-square (χ^2) error criterion which is mathematically represented as:

$$\chi^2(P) = \sum_{i=1}^{n} \left[\frac{X(t_i) - \hat{Y}(t_i,P)}{\sigma_{Y\,i}} \right]^2 \tag{4.8}$$

where, σ_{Yi} is the measurement error for measurement $Y(t_i)$.

We calculate RMSE of counter value as 5.238 (1.27mV) for $V_{in} < V_{IH}$, and $a = 2.238$, $b = 0.9233$ and $c = -79.69$ with 95 % confidence bounds.

Similarly for $V_{in} \geq V_{IH}$ RMSE and estimates of *a*, *b*, and *c* are 23.97 (5.85 mV) and 0.1526, 1.178 and 660.4 respectively. The linearized and the calibrated equations of the characteristics shown in Fig. 4.5 are:

$$y_i = 2.238 \cdot x_i^{0.9233} - 79.69 \text{ , for } V_{in} < V_{IH} \tag{4.9}$$

$$y_i = 0.1526 \cdot x_i^{1.178} + 660.4 \text{ , for } V_{in} \geq V_{IH} \tag{4.10}$$

The linearization error compensating scheme of equation (4.9-4.10) are implemented in a PIC µC by applying analog voltage from 0-V_{DD} . The compensation capability of the technique is depicted in Fig. 4.5.

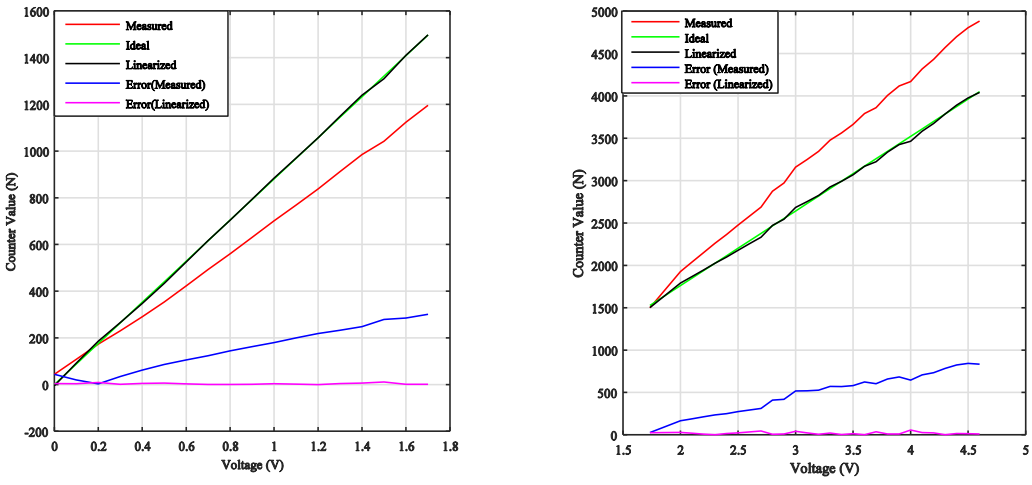

(a) (b)

Fig. 4.5. Error plot before and after error compensation (a) $N < N_0$ and (b) $N > N_0$.

It shows that for both the ranges of V_{in} ($V_{in} < V_{IH}$ and $V_{in} \geq V_{IH}$), the error of the measured values has been substantially reduced as evident from the error characteristics. Therefore we are able to faithfully represent the measured counter values in a linear mode corresponding to the input analog voltages by nADC approach. In succeeding section it will be justified that this computational technique will result a promising classification of gases in nADC approach.

4.3. Experimental Setup

As mentioned in chapter 3, a multisensory measurement system (shown in Fig. 4.6) was developed which consists of (a) sample and sensor chamber (b) gas sensor array, placed inside the sensor chamber (c) power supplies (d) pumps, valves and a mass flow controller (MFC) to control the gas and air circulation (e) µC, for data acquisition, control of gas flow system and linearization for error compensation, and (f) LCD displays to display the results. In contrast to the E-Nose system discussed in chapter 3, here online error compensation of DIC-based measurement is performed. Therefore, the µC based DIC is able to accurately measure the sensor responses in terms of counter value.

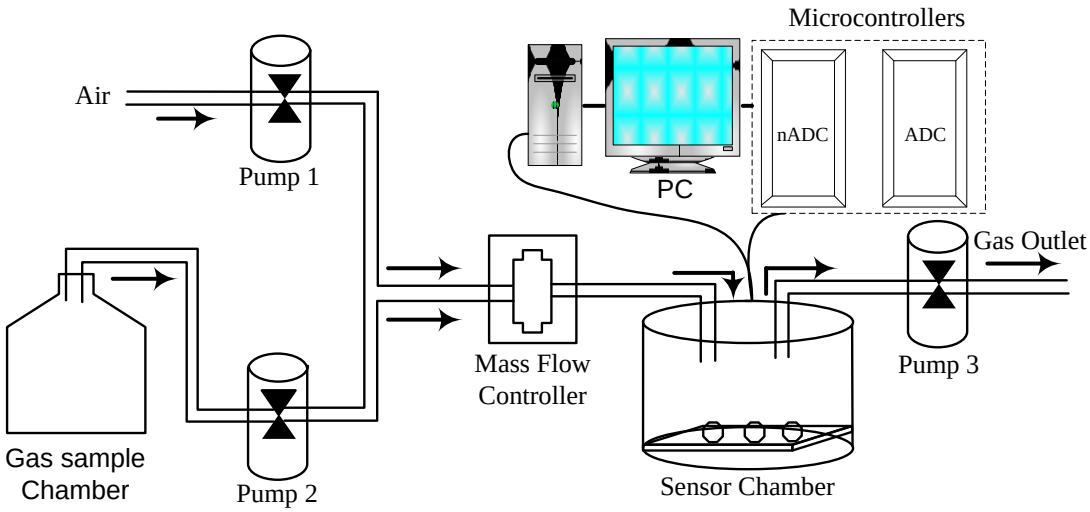

Fig. 4.6. Experimental setup of E-Nose.

Three commercial MOS gas sensors TGS 2620, TGS 832 and TGS 2201 from Figaro Engineering, Inc. (Osaka, Japan) are used as the array in the sensor chamber. The reason for selecting MOS gas sensors is their good cross-sensitivity, which facilitates detection of a wide variety of gases [31, 32]. A prior experimentation was conducted to select these three sensors from 6 sensors (TGS 822, TGS 825, TGS 832, TGS 2600, TGS 2620 and TGS 2201) due to their high sensitivity and selectivity to a wide variety of gases.

Moreover in [31] it has been demonstrated that with only four MOS gas sensors (TGS 2602, TGS 2620, TGS 2201A and TGS 2201B) classification accuracy as high as 89.9 in MLP and 100 % in HSVM has been obtained.

Similar to our earlier experiments discussed in chapter 3, in this work the sensor responses were collected at a constant room temperature (25 °C) and constant relative humidity (60±5%). Through experimentation the optimum response and purging time were determined and are found to be 80 s and 100 s respectively. The gas samples are prepared by injecting 300 µL of the liquid samples in the sample chamber and allowed to volatilize for about 10 min. The gas was transported from the sample chamber to the sensor chamber at a constant flow rate of 1.2 SLPM controlled by a MFC. On exposing the sensors to the gas sample the output responses of the sensors gradually increases and reaches a peak stable state, whereas on removal of gas and application of fresh air the sensor responses gradually decreases and reaches its baseline value. The sensor responses are acquired by the two identical µCs using ADC and nADC approaches. The response voltage data is transferred and stored via USB USART in a computer in ADC approach while counter values are stored in case of nADC, for further analysis.

Fig. 4.7 shows the sensor array interface to the two PIC µCs for nADC and ADC based measurements.

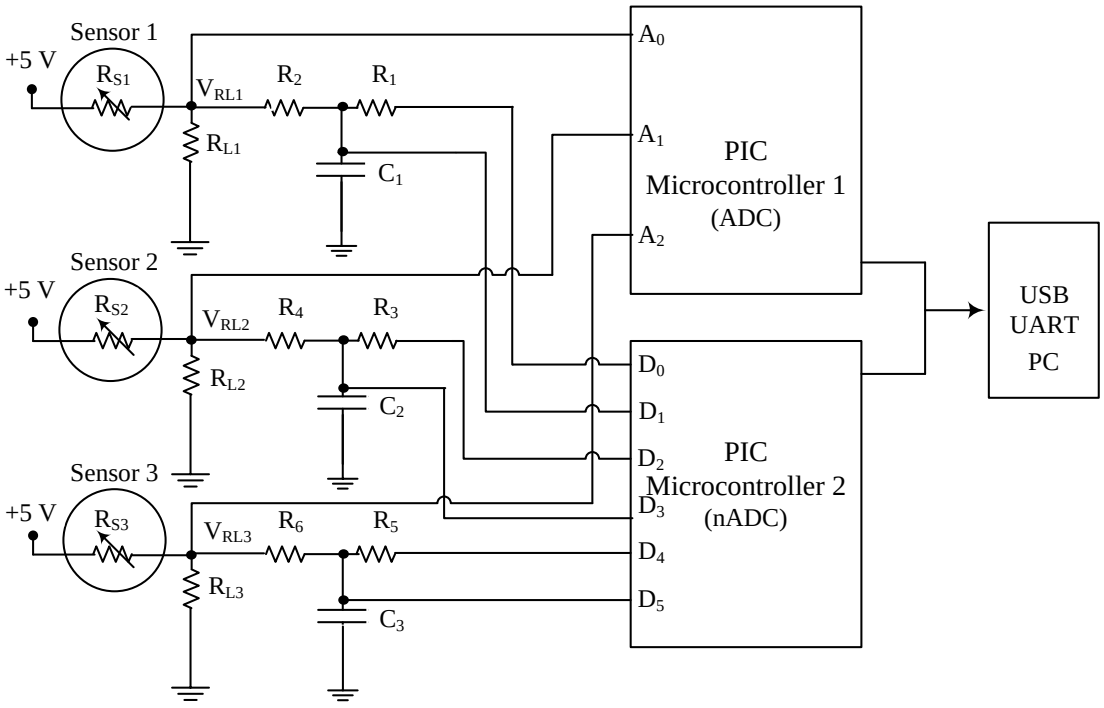

Fig. 4.7. nADC and ADC based measurement Circuit.

The study is conducted in two steps- in step 1 the stored data is processed in MATLAB for cluster analysis using PCA and offline classification of gases. In step-2 the classification models developed for ADC and nADC are coded in two µCs for online gas classification simultaneously.

4.4. Clustering and Classification

The nADC and ADC based features are compared using PCA and FFBP ANN in MATLAB. PCA is performed to check the cluster existence of the different gases used, whereas, FFBP ANN acts as the gas identification tool. We investigate the gas discrimination capability of both the systems for comparative analysis. The FFBP model used in both the cases is shown in Fig. 4.8, which consists of three layers- input layer, one hidden layer and output layer, where the subsequent layer has a connection from the preceding layer. The activation functions used in the input, hidden and output layer are tan-sigmoid log-sigmoid and purelin respectively. The input layer comprises of three neurons representing the three gas sensors, whereas the number of neurons at the output layer is set to one which represents the gas. The number of neurons at the hidden layer affects the discriminative capability of the ANN. For smaller number of hidden neurons the accuracy may not be adequate and too many hidden neurons may result in over fitting. Moreover, prior to training there are no formal methods to determine the number of hidden neurons. Therefore the ANN was trained with four numbers of hidden neurons- 1, 2, 3 and 4, using the Levenberg-Marquardt optimization technique.

For analysis and validation of the nADC driven E-Nose array we have acquired responses of three MOS gas sensors for four target gases. Each gas was sniffed by the sensors to generate 50 feature voltages which accounts to a total data size of $30\times4\times50$.

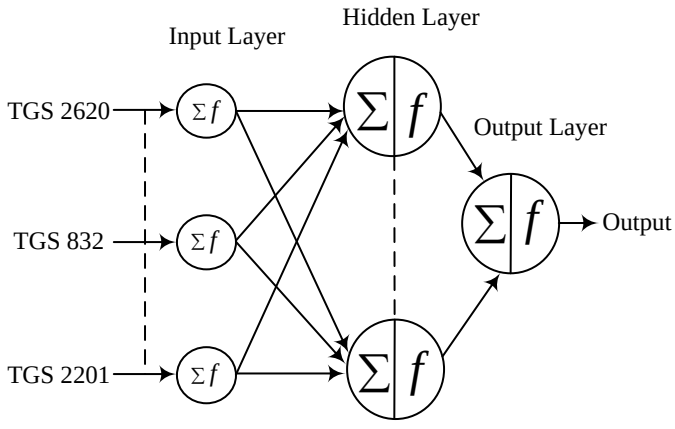

Fig. 4.8. ANN model.

4.5. Results and Discussion

4.5.1.Measurement system

The gas sensors' responses were measured by the internal ADC of the µC and by nADC technique and then linearized.

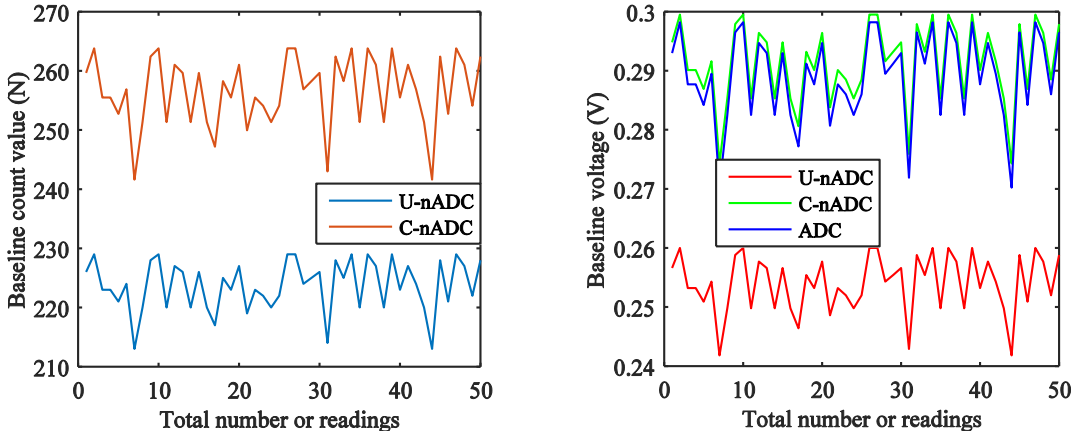

(a) (b)

Fig. 4.9. Baseline of TGS 2620 (a) count values and (b) voltage.

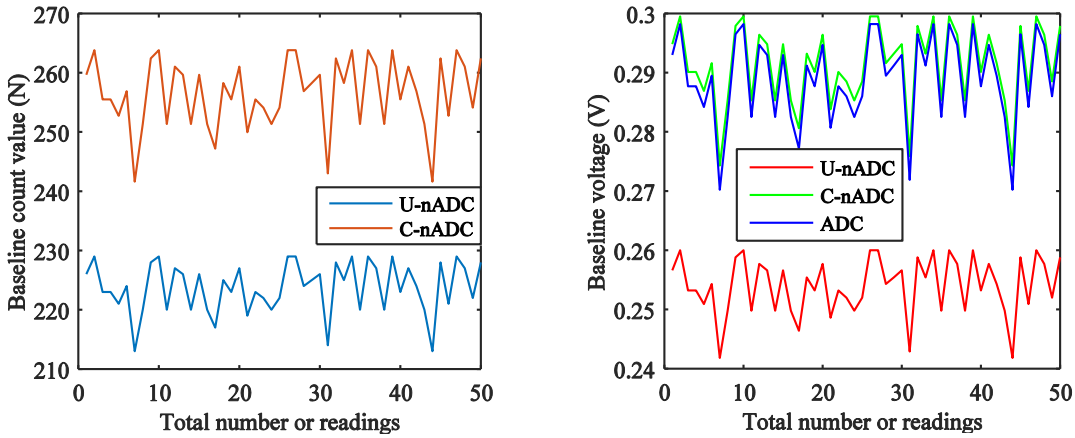

(a) (b)

Fig. 4.10 Baseline of TGS 832 (a) count values and (b) voltage.

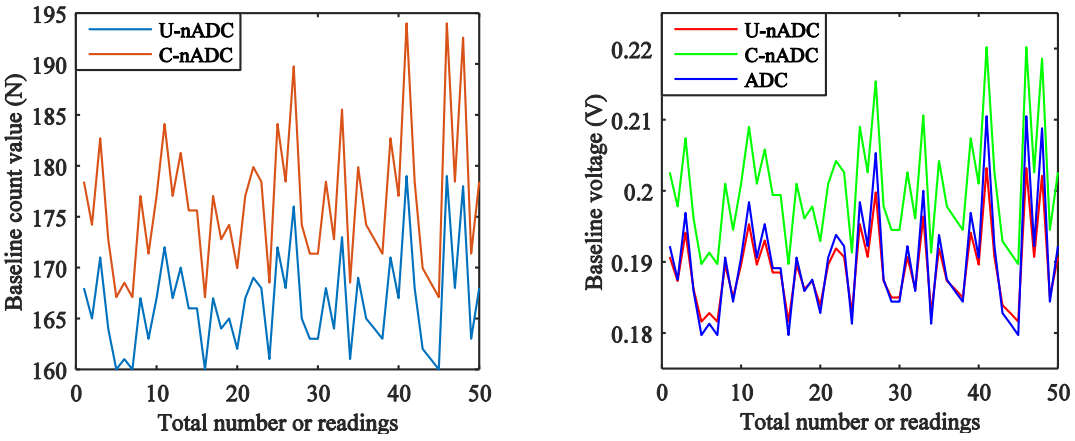

(a) (b)

Fig. 4.11 Baseline of TGS 2201 (a) count values and (b) voltage.

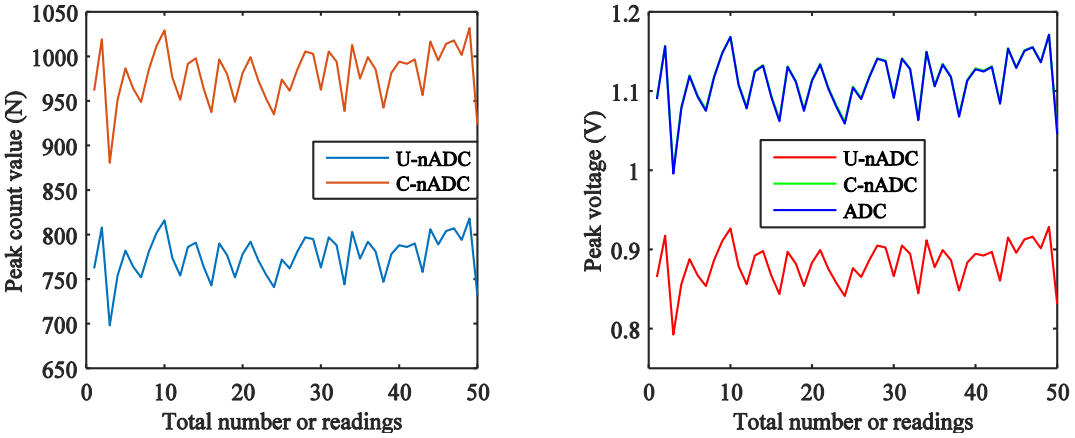

(a) (b)

Fig. 4.12 Peak of TGS 2620 to methanol (a) count values and (b) voltage.

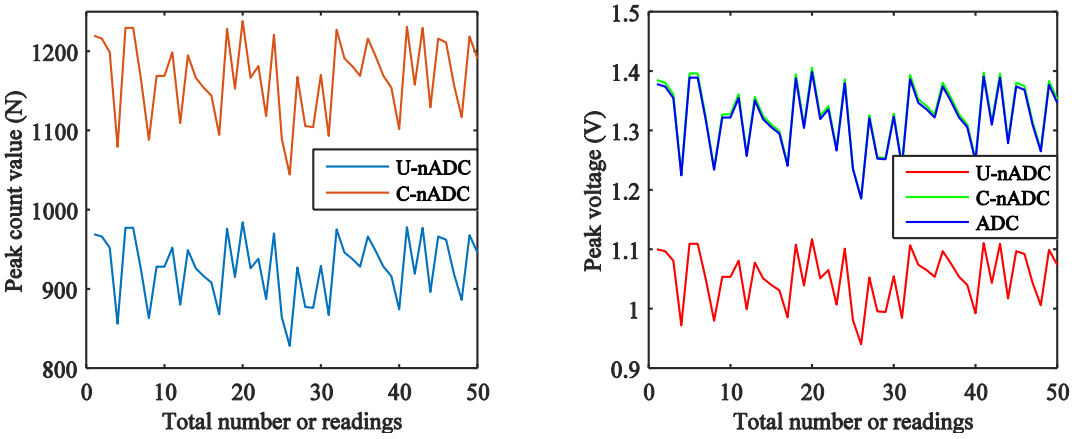

(a) (b)

Fig. 4.13 Peak of TGS 832 to methanol (a) count values and (b) voltage.

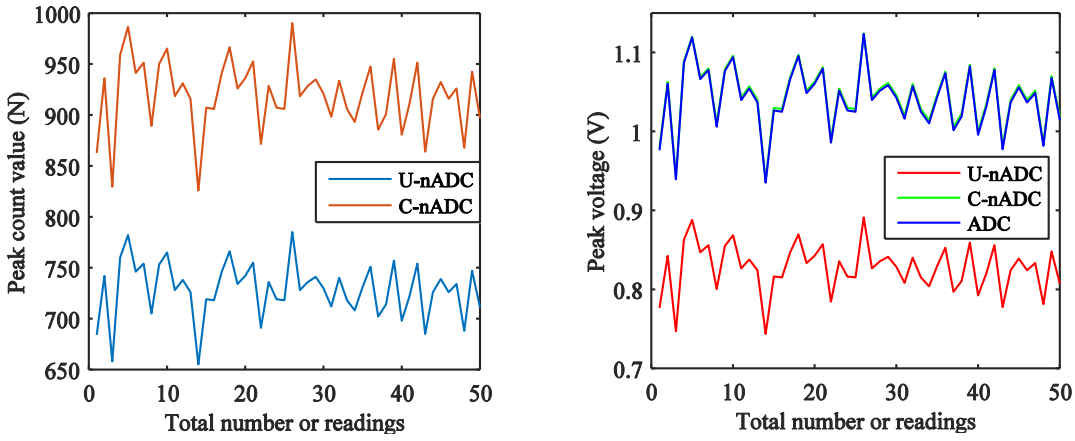

(a) (b)

Fig. 4.14 Peak of TGS 2201 to methanol (a) count values and (b) voltage.

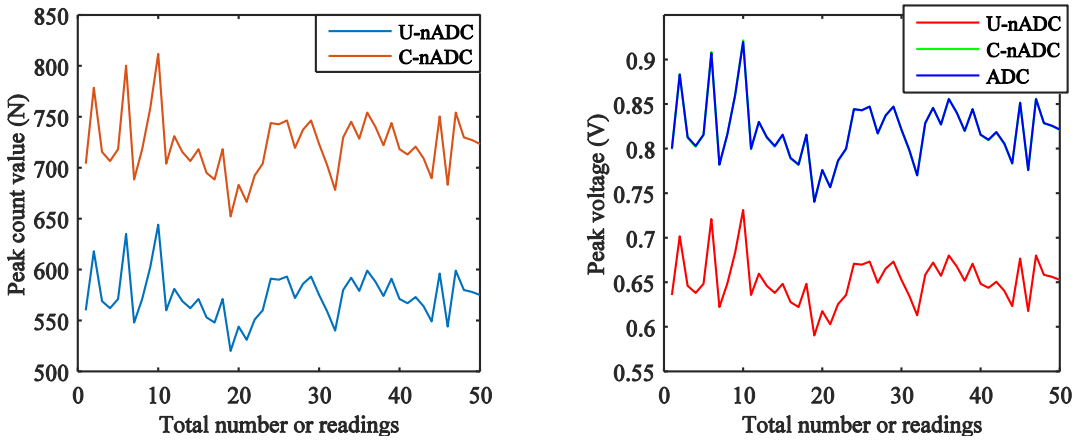

(a) (b)

Fig. 4.15 Peak of TGS 2620 to acetic acid (a) count values and (b) voltage.

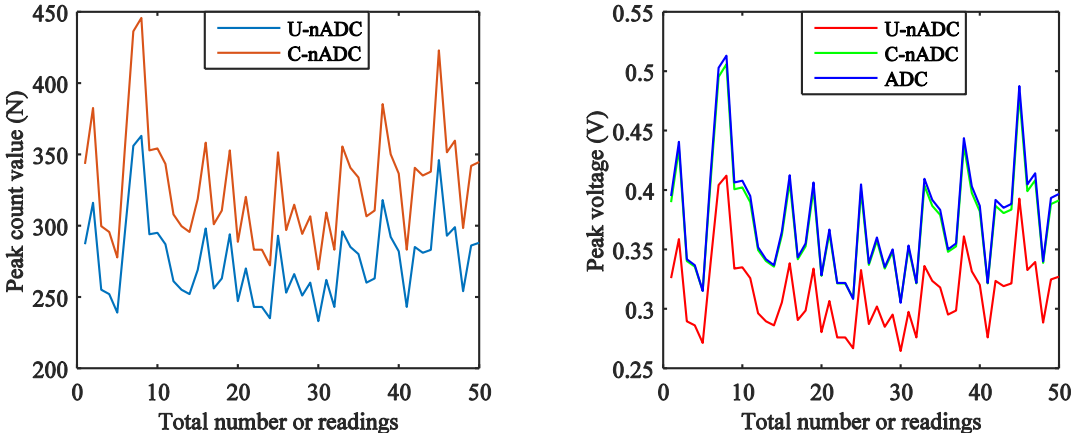

(a) (b)

Fig. 4.16. Peak of TGS 832 to acetic acid (a) count values and (b) voltage.

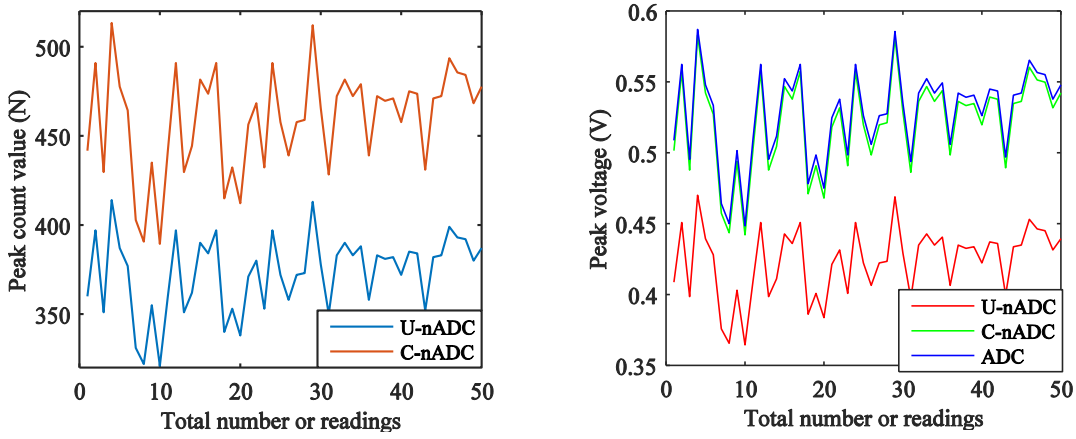

(a) (b)

Fig. 4.17. Peak of TGS 2201 to acetic acid (a) count values and (b) voltage.

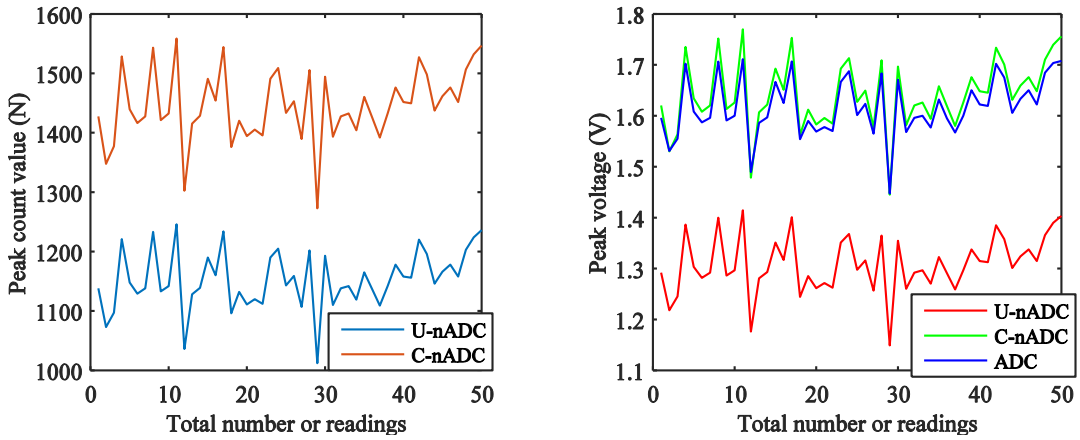

(a) (b)

Fig. 4.18. Peak of TGS 2620 to acetone (a) count values and (b) voltage.

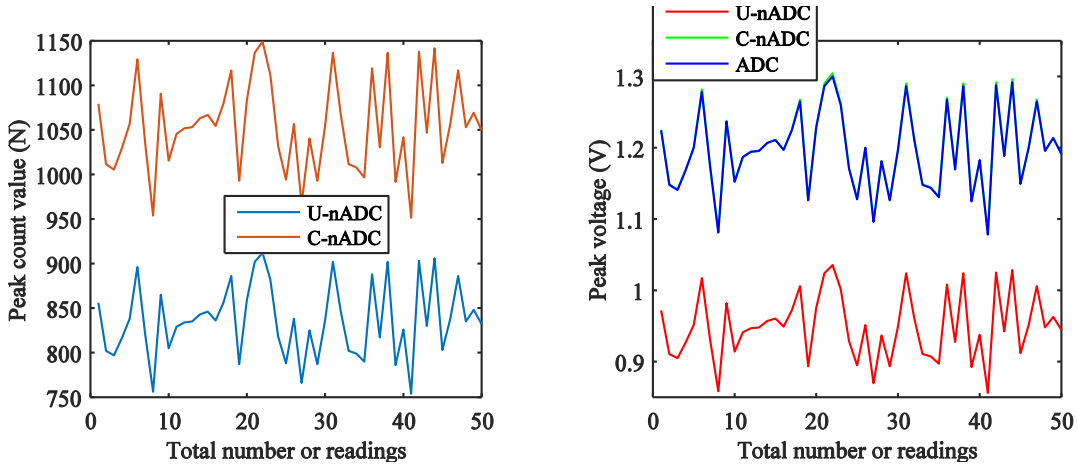

(a) (b)

Fig. 4.19. Peak of TGS 832 to acetone (a) count values and (b) voltage.

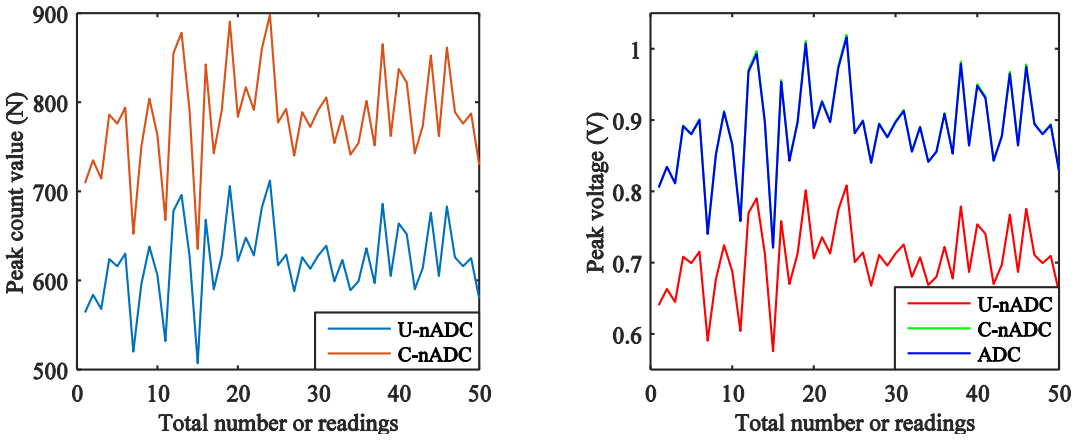

(a) (b)

Fig. 4.20. Peak of TGS 2201 to acetone (a) count values and (b) voltage.

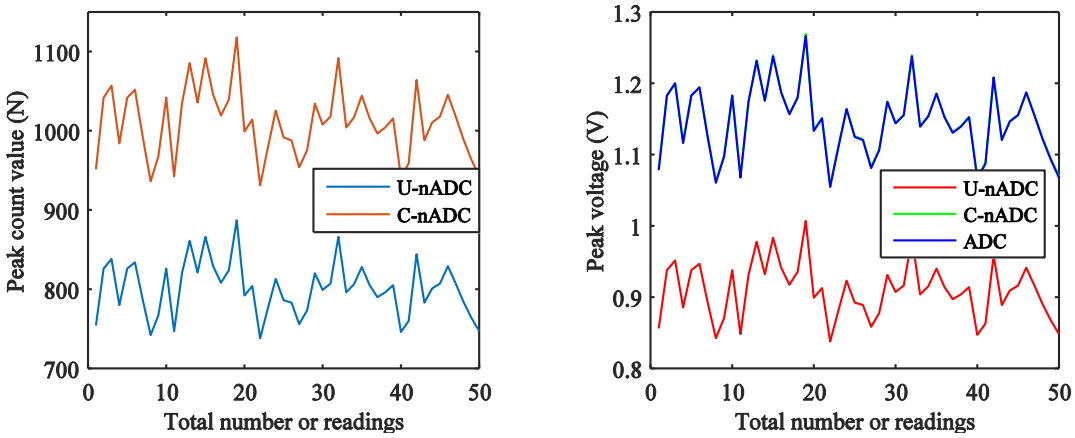

(a) (b)

Fig. 4.21. Peak of TGS 2620 to 2-propanol (a) count values and (b) voltage.

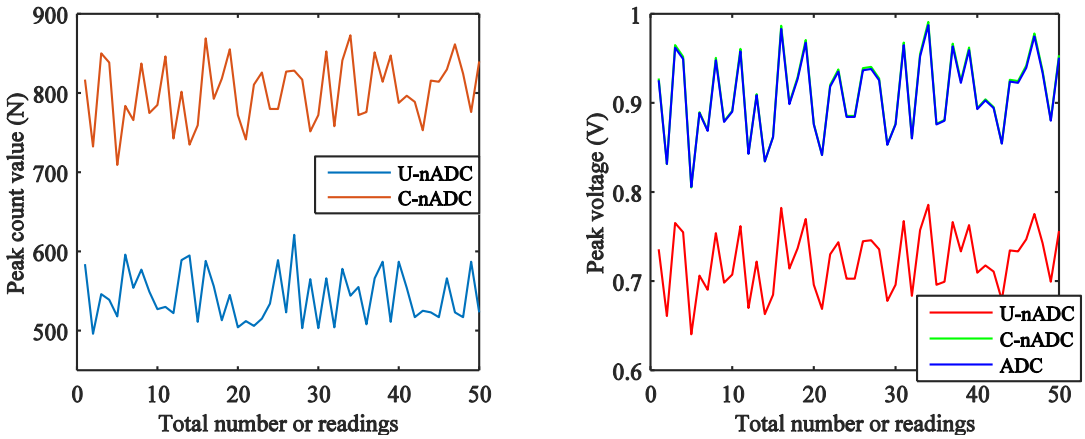

(a) (b)

Fig. 4.22 Peak of TGS 832 to 2-propanol (a) count values and (b) voltage.

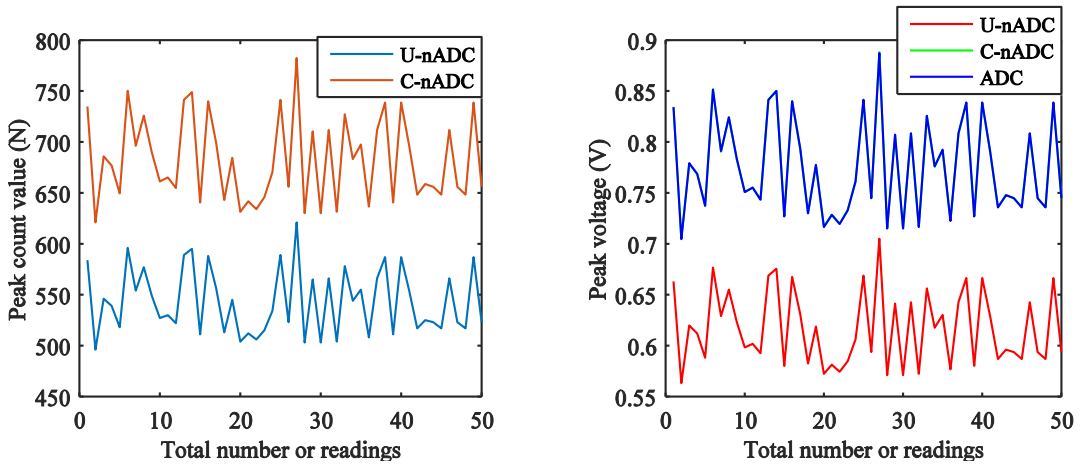

(a) (b)

Fig. 4.23. Peak of TGS 2201 to 2-propanol (a) count values and (b) voltage.

The count values and their corresponding voltages of the peak and baseline of the sensors responses on application and removal of various gases are collected by the µC. The collected values transferred to the computer via USB UART are illustrated in Fig 4.9-4.23. Since for all the target gases, the peak value of the sensors for inbuilt ADC and C-nADC are almost the same therefore in the figures they merge with one another. It is notable from the repeatability plots that there are small jumps in the peak and the baseline values of the different sensors, however, the error is sufficiently small and does not affect the predictive accuracy of the system.

The outputs from the µC were transferred to a PC via USB UART at a baud rate of 9600 bps. The USB-UART connection is accomplished using a FT232RL IC, which provides USB to serial UART interface. Table 4.2 shows the mean values of the data set for the three sensors with their standard error of mean (SEM). We present in this work the comparison of measured responses among three approaches- with inbuilt µC ADC, error compensated nADC (C-nADC) and uncompensated nADC (U-nADC). It is observed in C-nADC and ADC that the maximum deviation is in case of TGS 2620 (0.02 V) for G3 and the minimum deviation is of TGS 2201 (0.0001 V) for G4. Whereas the measurements performed considering U-nADC results in high amount of error compared to that of the inbuilt ADC of the µC**.** It can be inferred from Table 4.2 that due to close approximation of the inbuilt ADC and C-nADC to that of an ideal ADC their responses are within a close range. However, in case of the U-nADC a wide variation in responses compared to C-nADC and ADC is observed. Therefore as aforementioned, the response patterns from the sensors are appropriately captured using C-nADC and ADC based methods.

Table 4.2 Comparison of linearized counter values and voltages.

Sensors	Baseline			Gas	Peak				
	ADC	U-nADC	C-nADC		ADC	U-nADC		C-nADC	
	Mean ± S.E.M (V)	Mean ± S.E.M (N)	Mean ± S.E.M (N)		Mean ± S.E.M (V)	Mean ± S.E.M (N)	Mean ± S.E.M (V)	Mean ± S.E.M (N)	Mean ± S.E.M (V)
TGS 2620	0.2889 ± 0.0005	256.76 ± 0.49	302.054 ± 0.491	G1	1.1109 ± 0.0049	776.64 ± 3.37	0.8819 ± 0.0038	979.8 ± 4.28	1.1126 ± 0.0049
				G2	0.8197 ± 0.0048	573.98 ± 3.34	0.6518 ± 0.0038	721 ± 4.31	0.8187 ± 0.0049
				G3	1.6175 ± 0.0082	1153 ± 6.99	1.3093 ± 0.0079	1445.6 ± 8.53	1.6415 ± 0.0097
				G4	1.1461 ± 0.0070	801.06 ± 4.87	0.9096 ± 0.0055	1010.4 ± 6.11	1.1473 ± 0.0069
TGS 832	0.1896 ± 0.0007	176.42 ± 0.58	190.363 ± 0.580	G1	1.3204 ± 0.0077	926.78 ± 5.62	1.0524 ± 0.0064	1167.3 ± 6.98	1.3225 ± 0.0079
				G2	0.3768 ± 0.0067	276.46 ± 4.15	0.3139 ± 0.0047	328.82 ± 5.64	0.3734 ± 0.0064
				G3	1.1959 ± 0.0081	836.2 ± 5.81	0.9495 ± 0.0066	1054.4 ± 7.27	1.1973 ± 0.0083
				G4	0.9086 ± 0.0063	636.20 ± 4.44	0.7224 ± 0.0051	801.8 ± 5.68	0.9105 ± 0.0064
TGS 2201	0.3304 ± 0.0014	297.72 ± 1.00	357.88 ± 1.001	G1	1.0406 ± 0.0057	728.46 ± 3.88	0.8272 ± 0.0044	919.0 ± 4.91	1.0436 ± 0.0056
				G2	0.5276 ± 0.0045	373.22 ± 3.04	0.4238 ± 0.0035	459.23 ± 4.06	0.5215 ± 0.0046
				G3	0.8875 ± 0.0088	621.5 ± 6.17	0.7057 ± 0.0070	782.9 ± 7.91	0.8890 ± 0.0090
				G4	0.7747 ± 0.0067	543.36 ± 4.59	0.6170 ± 0.0052	682.3 ± 5.93	0.7748 ± 0.0067

To justify the novelty of our proposed method we present here the comparison with the state of the art techniques in Table 4.3. Various topologies of DIC have been proposed for accurate measurement of sensor response measurement since 2005. For the measurement of change in resistance or capacitance of a sensor three different topologies are reported in literature namely single, differential and full bridge topology. In all the topologies a three-signal-auto-calibration technique is applied to measure the sensor output. However, in this technique, it is necessary to measure three discharge time, which is time-consuming. Moreover, to measure a single sensor response at least 4 separate µC pins are required. In contrast, the technique presented here requires only two pins to measure the sensor response. Moreover, error compensation after measurement of sensor response is only available in our proposed technique.

Table 4.3 Comparison with state of the art techniques.

Methods	Microcontroller Used	Topology	Measured Quantity	Complexity Level	Multisensory Environment	Nonlinearity Error %	Error Compensation after measurement
[20]	PIC16F873	Single topology	Resistance	Medium	No	0.01% FSS	No
[23]	AVR ATtiny2313	Differential topology	Resistance	High	No	0.01% FSS	No
[27]	MSP430F123	Full-bridge topology	Resistance	High	No	1.8% FSS	No
[24]	AVR ATtiny2313	Single topology	Capacitance	Medium	No	2% FSS	No
[25]	AVR ATtiny2313	Differential topology	Capacitance	High	No	1.1% FSS	No
[3]	PIC 18F458	Single topology	Analog Voltage	Low	No	-	No
[9]	PIC 18F45K22	Single topology	Analog Voltage	Low	Yes	< 0.2%	No
Proposed Work	PIC 18F45K22	Single topology	Analog Voltage	Low	Yes	< 0.01%	Yes

From the error compensation analysis it is evident that the proposed technique is able to compensate the nonlinearity with less than 0.01% error which is distinctly found to be a better method. Therefore we propose to preprocess the data with the technique for classification of the gases as discussed below.

4.5.2.Clustering and classification

To analyze the correlation of the sensor responses for different gases PCA is used. Principal component analysis (PCA), which is an unsupervised multivariate pattern clustering method, represents the original dataset with a new set of linear orthogonal variables called principal components (PCs). We have normalized the data set (each sensor

for each gas) by dividing the data by its corresponding maximum value. We project the four gases on the first three PCs (Fig. 4.24), since they accounted for more than 99% of the cumulative contribution of variance. The PCA shows good cluster separation among the two gases. It is observed that there is a partial overlapping between clusters of methanol and acetone (Fig. 4.24 (c)).

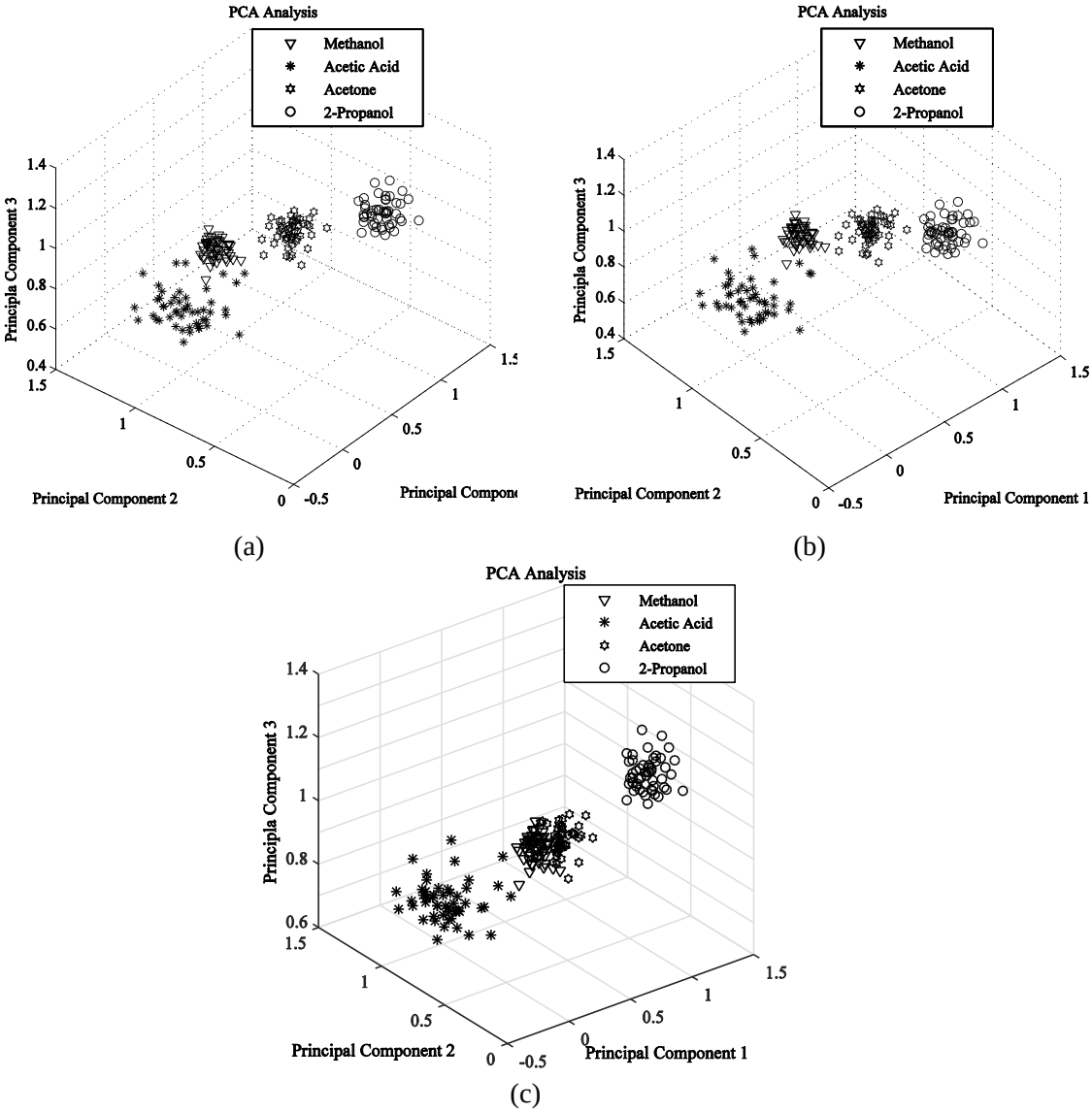

Fig. 4.24. PCA of (a) U-nADC, (b) C-nADC and (c) ADC based approaches.

As mentioned in chapter 3, PCA plot can only provide us a visual aid for observing the cluster separation a quantitative metric- inter-intra class distance ratio is measured to quantify the separation of clusters in a 3-D space. In pattern classification, the data objects

are better clustered if the cluster members have lower intra-class distance and higher inter-class distance [14]. The Euclidean intra-class distance (d_{intra}), inter class (d_{inter}) distance and inter-intra class distance ratio for a particular gas cluster is determined using equations (3.16), (3.17) and (3.18), presented in chapter 3.

Table 4.4 shows the Euclidean intra-class distance calculated for the four gas clusters. The highest intra-class distance is observed in case of acetic acid, which yields 0.1827, 0.1812 and 0.1789 using U-nADC, C-nADC and ADC respectively.

Table 4.5 shows the Euclidean inter class distance between all the four gas clusters. We have further, determined the Euclidean inter-intra class distance ratio to obtain a single measure of class separation (Table 4.6) for all the classes.

The average intra-class distance, inter-class distance and the class distance ratio of the entire dataset were calculated and found to be almost equal for C-nADC and ADC. The inter-intra class distance ratio of the entire cluster dataset is shown in Table. 4.7, it is confirmed from Table 4.4-4.7 that the proposed method of direct interfacing conforms to that of ADC based approach in case of cluster classification.

Table 4.4 Euclidean intra class distance.

Gas	U-nADC	C-nADC	ADC
Methanol (G1)	0.0743	0.0718	0.0719
Acetic Acid (G2)	0.1827	0.1812	0.1789
Acetone (G3)	0.1058	0.1026	0.0965
Propanol (G4)	0.1128	0.1100	0.1101

Table 4.5 Euclidean inter class distance for nADC and ADC.

Method	G1G2	G1G3	G1G4	G2G3	G2G4	G3G4
U-nADC	0.7637	0.4334	1.1013	0.9174	1.919	0.7079
C-nADC	0.7876	0.3640	1.0433	0.9231	1.1933	0.7181
ADC	0.8281	0.2607	1.0215	0.8990	1.2414	0.7706

Table 4.6 Euclidean inter-intra class distance ratio for nADC and ADC.

(a) U-nADC

	G1	G2	G3	G4
G1	0	10.278	5.833	14.822
G2	4.180	0	5.021	6.523
G3	4.096	8.671	0	6.690
G4	9.763	10.566	6.275	0

(b) C-nADC

	G1	G2	G3	G4
G1	0	10.969	5.069	14.530
G2	4.346	0	5.099	6.585
G3	3.547	8.997	0	6.990
G4	9.493	10.848	6.528	0

(c) ADC

	G1	G2	G3	G4
G1	0	10.9541	5.0626	14.5104
G2	4.4025	0	5.1599	6.6702
G3	3.7720	9.5658	0	7.4415
G4	9.4850	10.8383	6.5233	0

Although PCA and Euclidean inter-intra class distance ratio provides a better understanding about the clusters formation of the four gases, the clustering is unsupervised and classification cannot be performed using this technique. It is observed that between n-ADC techniques, C-nADC provides more accurate measurement compared to U-nADC, so we have evaluated the effect of error compensation on the classification accuracy. Further, performance of ANN for ADC, U-nADC and C-nADC is compared and shown in Table 4.8. In order to classify gas samples we have used FFBP ANN. The feature datasets of the three approaches are partitioned as- 60% for training and 40% for testing. The number of hidden neurons (n) for the best classification performance is found to be 4 for implementation in ADC as well as for U-nADC and C-nADC (Table 4.8). It is observed that C-nADC results in higher classification accuracy (98.75%) than that of U-nADC (97.91%) and ADC (97.08%) in our multisensory environment. The weights and biases of the neural networks with optimal hidden neurons simulated in MATLAB are used to code the ANN algorithm in two separate µCs for online comparison of the proposed method. In one µC both the U-nADC and C-nADC based prediction results are calculated sequentially and displayed in a LCD, and in the other µC ADC based prediction is performed. The µC based observation is depicted in a confusion matrix as shown in Table 4.9.

Table 4.7 Class distances of the entire dataset

Parameters	U-nADC	C-nADC	ADC
Average Inter-Class distance	0.8526	0.8382	0.8368
Average Intra-Class distance	0.1189	0.1164	0.1144
Inter-Class/Intra-Class distance ratio	7.1707	7.2010	7.3170

Table 4.8 ANN Count performance parameters with varying hidden neurons

Data Size	Hidden	Time (s)			No. of Epochs			Accuracy (%)			Mean Square Error (M.S.E.)		
	Neuron (n)	ADC	U-nADC	C-nADC	ADC	U-nADC	C-nADC	ADC	U-nADC	C-nADC	ADC	U-nADC	C-nADC
$4\times100\times3$	1	2.49	2.24	2.24	3	4	3	25	25	50	1.5	1.50	1.25
	2	2.33	2.44	5.64	9	6	265	48.33	50	72.5	0.658	0.50	0.283
	3	2.27	2.49	29.96	7	13	2226	50	50	95.83	0.500	1.2250	0.250
	4	14.84	2.65	2.525	1000	18	18	97.08	97.91	98.75	0.008	0.0008	0.00056

The nADC and ADC based online gas discrimination of 200 gas samples (50 samples for each gas) analyzed accounted for 95%, 96.5% and 98% accuracy for ADC, U-nADC and C-nADC respectively.

Table 4.9 Confusion matrix showing online performance of (a) ADC, (b) U-nADC and (c) C-nADC.

(a)

Actual output \ Predicted output	G1	G2	G3	G4	
G1	43	0	7	0	86%
G2	0	50	0	0	100%
G3	3	0	47	0	94%
G4	0	0		50	100%
	93.47%	100 %	87.03%	100%	95%

(b)

Actual output \ Predicted output	G1	G2	G3	G4	
G1	44	0	6	0	88%
G2	0	50	0	0	100%
G3	1	0	49	0	98%
G4	0	0		50	100%
	97.77%	100 %	89.09%	100%	96.5%

(c)

Actual output \ Predicted output	G1	G2	G3	G4	
G1	47	0	3	0	94%
G2	0	50	0	0	100%
G3	1	0	49	0	98%
G4	0	0		50	100%
	97.91%	100 %	94.23%	100%	98%

It is experimentally found that although overleaping clusters are formed in PCA of ADC framework, the testing accuracy of the ADC framework is only 3% less than as that of C-nADC. This is due to the fact that unsupervised linear model such as PCA may sometime fail to provide a complete solution to the classification problem. However, the use of supervised non-linear model such as FFBP ANN could provide good predictive accuracy, even if overlapping cluster exists in PCA [5]. It is worth mentioning that the performance of ANN-based learning depends on appropriate setting of model parameters which are obtained by iterative training of the input features. However, the learning efficiency in terms of low processing time, minimum number of epoch, error function (i.e., MSE) relies on discriminant features of multiple input sources that to be identified. In case of low

discrimination among multiple groups' features which are embedded into single form of input vectors, the learning process becomes time consuming and requires more number of iterations to achieve an optimum level of MSE. Despite low Euclidean inter-class distance specifically for G1G3 in ADC method, the performance was not bad due to distinct parameter value that helps quick learning of the discriminant process. The low parameter value is presumably due to the fact that built-in ADC resolution is 10-bit while nADC measurements have a resolution of 12-bit. As is evident, the learning with C-ADC was achieved at less number of epochs for smaller time interval as compared to that of the ADC. A small difference in error is observed, however, it is reasonable to achieve small difference of performance.

The scalability of the proposed approach is also examined in the context of results obtained using the optimized model on new set of data that has not been previously used for this measurement [13]. In order to investigate the systems scalability the system is trained with the new dataset of the gas sensor responses and testing was performed. The experimentation is repeated for three cycles and accordingly performances have been investigated which is found to be satisfactory. The quantitative measure achieved in terms of average accuracy for ADC, U-nADC and C-nADC are found to be 94.66%, 96.833 and 98.16% respectively. Thus it ensures the robustness and viability of the proposed system for real time measurement.

We admit that number of pins in a µC rules the number of signals which in turn rules the cost of the package. As in our proposed approach two spare input lines are required for each analog signal, the system may not be feasible when the number of sensors in an array is very large. However, a noteworthy merit of this approach is multisensory response measurement and application of online discrimination algorithms in µC is achieved by using simple off-the-shelf components.

4.6. Measurement Uncertainty

In spite of accurate and precise measurement of sensor signals using most sophisticated instruments, the interpretation is not always ideal. Different measurement characteristics includes- accuracy, precision, repeatability, resolution etc. Uncertainty is another metric of measurement systems. The imperfection inherent in measuring real world measurements is

called uncertainty. This flaw may be due to limitations of the measuring instrument, measurement process, imported uncertainty, operator skill, sampling issue and the environment [1, 2]. Measurement uncertainty is a non negative parameter that investigates the individual uncertainty in measurement of various parameters that contributes to the final uncertainty of the measurand. Here we will analyze the various parameters contributing to the uncertainty in measurement of the DIC based E-Nose sensor response voltages (V_{RL1}, V_{RL2} and V_{RL3}) for the three sensors used; the estimated concentration levels of the gases and the local circuit parameters. Typically the measurand and the parameters contributing to its uncertainty can be expressed in a mathematical model that provides us the necessary tool to measure the final uncertainty.

Let us define the measurand as, $Y = f(X_1, X_2, X_3.....)$ where, X_i is the number of parameters contributing to uncertainty in Y. To determine the standard uncertainty of different parameters two types of estimations are adopted. Standard uncertainty (U) estimation of the mean, for a repeated number of readings of the parameter with standard deviation (S) is determined using [1, 2] –

$$U(X_i) = \frac{S}{\sqrt{n}} \tag{4.11}$$

where, $s = \sqrt{\frac{\sum_{i=1}^{n}(X_i - \overline{X})^2}{n-1}}$, $\overline{X}$ is the mean, n is the number of measurements of the parameter and X_i is the measurand.

In cases where we are only able to establish the upper and lower bounds of uncertainty, we consider the parameters to be in rectangular distribution with uncertainty [1, 2] given by-

$$U(X_i) = \frac{a}{\sqrt{3}} \tag{4.12}$$

where, a is the half-width between upper and lower limits of uncertainty. The overall uncertainty of the measurand is given by [1, 2]-

$$U(Y) = \sqrt{\sum_{all\ i}(S_i \times U(X_i))^2} \tag{4.13}$$

where, the sensitivity is given by-

$$S_i = \frac{\partial f}{\partial X_i} \tag{4.14}$$

In this work we propose to estimate the uncertainty caused by the sensor circuit and DIC parameters in measurement of output responses from a MOS gas sensor array.

4.6.1.Uncertainty estimation

There is a certain amount of uncertainty in the measurement of sensor response voltage (V_{RL}) due to uncertainty of the sensor circuit parameters and that of the DIC parameters. The parameters measured using the digital multimeter (keithley 2110), consists maximum deviation within the range (distribution limit) of ± 0.5, therefore equation (4.12) is used to find their uncertainty contribution.

We are analyzing this in two steps. First the gas concentration dependent sensor response in resistance (R_S) is given by (4.15)

$$R_S = A \times [C_n]^{-\alpha} \tag{4.15}$$

where, A is a concentration independent constant, C_n is the concentration of the gas and α is the exponent of the power law dependent on the gas. The response voltage of the sensor across the load resistance is given in (3.11), in chapter 3. Now combining (4.15) and (3.11), it is proposed that-

$$V_{RL} = \frac{V_C \times R_L}{A \times C_n^{-\alpha} + R_L} \tag{4.16}$$

This equation accounts for the dependency of both the sensor and gas parameters on the response voltage. However the exponent α can be related to depletion theory of the semiconductor surface and the chemistry of the gas adsorption reaction [30]. Further, α is found to dependent on the W/L ratio of the semiconductor [30]. Therefore the values of α will be different for different sensors for a particular gas.

In order to determine the uncertainty of the local sensor parameters of (4.16), the value of α should be known. The values of α is typically calculated by measuring the sensitivity of the sensor at two different concentrations using –

$$\alpha = \frac{\log(R_{S2}) - \log(R_{S1})}{\log(C_{n2}) - \log(C_{n1})} \tag{4.17}$$

Web-based computational engine WolframAlpha [29] was used to obtain the solution of the differential equation to estimate the sensitivity coefficients of individual sensor parameters in equation (4.16). The sensitivity coefficients of individual parameters are calculated using (4.18-4.21) as:

Sensitivity of V_C *:*

$$S_{V_C} = \frac{\partial V_{RL}}{\partial V_C} = \frac{\partial}{\partial V_C}\left(\frac{V_C \times R_L}{A \times C_n^{-\alpha} + R_L}\right)$$

$$S_{V_C} = \frac{R_L \times C_n^{\alpha}}{A + \left(R_L \times C_n^{\alpha}\right)} \tag{4.18}$$

Sensitivity of R_L *:*

$$S_{R_L} = \frac{\partial V_{RL}}{\partial R_L} = \frac{\partial}{\partial R_L}\left(\frac{V_C \times R_L}{A \times C_n^{-\alpha} + R_L}\right)$$

$$S_{R_L} = -\frac{V_C \times A \times C_n^{\alpha}}{\left(A + \left(R_L \times C_n^{\alpha}\right)\right)^2} \tag{4.19}$$

Sensitivity of C_n *:*

$$S_{C_n} = \frac{\partial V_{RL}}{\partial C_n} = \frac{\partial}{\partial C_n}\left(\frac{V_C \times R_L}{A \times C_n^{-\alpha} + R_L}\right)$$

$$S_{C_n} = -\frac{A \times \alpha \times R_L \times V_C \times C_n^{\alpha-1}}{\left(A + \left(R_L \times C_n^{\alpha}\right)\right)^2} \tag{4.20}$$

Sensitivity of α *:*

$$S_{\alpha} = \frac{\partial V_{RL}}{\partial \alpha} = \frac{\partial}{\partial \alpha}\left(\frac{V_C \times R_L}{A \times C_n^{-\alpha} + R_L}\right)$$

$$S_{\alpha} = -\frac{R_L \times V_C \times A \times C_n^{\alpha} \times \log(C)}{\left(A + \left(R_L \times C_n^{\alpha}\right)\right)^2} \tag{4.21}$$

The overall uncertainty is estimated using (4.13) as:

$$U(Y) = \sqrt{\left(S_{V_C} \times U\left(X_{V_C}\right)\right)^2 + \left(S_{R_L} \times U\left(X_{R_L}\right)\right)^2 + \left(S_{C_n} \times U\left(X_{C_n}\right)\right)^2 + \left(S_\alpha \times U\left(X_\alpha\right)\right)^2} \quad (4.22)$$

In the second step the dependency of the sensor response voltage on the direct-interface local parameters is derived as-

$$V_{RL} = (V_{IH}(R_1 + R_2) - R_2 \cdot V_{DD}(1 - e^{b_z})) \cdot (R_1 + R_2 \cdot e^{b_z})^{-1} \quad (4.23)$$

where, $b_z = -(1/C) \cdot ((1/R_1) + (1/R_2)) \cdot (N_0 - N) t_{loop}$

This equation is based on the condition that $V_{RL} < V_{IH}$ in our work, since the values of sensor responses $(V_{RL1}, V_{RL2}, V_{RL3})$ in all three gas sensors were found to be less than V_{IH} for the four tested gases. Similar to the estimation of uncertainty contributed by the local sensor parameter, the overall uncertainty in the measurement of V_{RL} is also estimated using (4.13).

4.6.2.Results and discussion

Under standard conditions the standard uncertainty of the gas flow chamber is determined as illustrated in Table 4.10. The standard uncertainty of the pipette used is provided by the manufacturer as 0.0173 ml. Therefore, for each gas, the standard uncertainty is 0.0173 ml, which is converted to their respective ppm level using equation (3.14), presented in chapter 3.

Table 4.10 Standard uncertainty of gas concentration (C_n).

Gas	Molecular weight (g/mol)	Density of liquid (g/ml)	Volume of liquid	Uncertainty of the pipette	Volume of gas flow Chamber	Standard uncertainty
Methanol	32.04	0.792	0.2 ml	0.0173 ml	557 ml	18.2700
Acetic Acid	60.05	1.049				12.9113
Acetone	58.05	0.791				10.0660
2-Propanol	60.01	0.786				9.6662

To estimate the uncertainty associated with α, for each tested gas, the values of α were determined by taking two data points in the power law characteristics- (R_{S1}, C_{n1}) and (R_{S2}, C_{n2}) where R_{S1} and R_{S2} are the sensor resistances when the gas with concentration level of C_{n1} and C_{n2} were applied. For each gas, 0.2 ml and 0.3 ml of the liquid were taken in a

fixed volume sample chamber of 280 ml, the concentration C_{n1} and C_{n2} were obtained as shown in (Table 4.11). The uncertainty in α was calculated by using (4.11) for $n = 5$ trials for all the gases as shown in Table 4.11-4.14.

It is observed that TGS 2201 yields the higher value of R_S for methanol, acetone, and 2-propanol and TGS 2620 for acetic acid. Further, the lower value of R_S is observed in case of TGS 832 for methanol, TGS 2201 for acetic acid and TGS 2620 for acetone and 2-propanol. As mentioned in chapter 1, higher the value of R_S lower is the sensitivity of the sensor towards the target gas and vice versa. It can be inferred from Table 4.11-4.14 that TGS 2620 is highest sensitive towards acetone then 2-propanol, methanol, and acetic acid respectively. Further, the decreasing order of sensitivity of TGS 832 is towards methanol, acetone, acetic acid and 2-propanol and TGS 2201 is towards 2-propanol, acetone, acetic acid, and methanol respectively.

It is worth mentioning the fact that uncertainty in E-Nose presents the errors propagating from the input gas parameters through the DIC to the output responses. Therefore, the efficiency of the E-Nose relies not only on the DIC parameters but also on the sensor local parameters such as gas concentration, exponent of power law of gas, and therefore the uncertainties associated with these parameters and their estimations and control are of paramount importance.

Table 4.11 Standard uncertainty of α in case of methanol.

Sensor	C_{n1} (ppm)	C_{n1} (ppm)	R_{S1} KΩ	R_{S2} KΩ	α	Standard Uncertainty
2620	211.2141	316.8212	2.1000	1.6418	-0.6071	0.0308
			2.1166	1.6742	-0.5784	
			2.1570	1.6465	-0.6661	
			2.2526	1.8613	-0.4706	
			2.1913	1.8034	-0.4804	
832			1.8560	1.2611	-0.9531	0.0717
			1.8728	1.3002	-0.9000	
			1.9642	1.2662	-1.0828	
			1.9642	1.4866	-0.6871	
			1.9174	1.4190	-0.7423	
2201			2.9030	2.4417	-0.4269	0.0170
			2.9896	2.4603	-0.4805	
			2.9222	2.4766	-0.4080	
			3.2287	2.7539	-0.3923	
			3.1436	2.6890	-0.3852	

Table 4.12 Standard uncertainty of α in case of acetic acid.

Sensor	C_{n1} (ppm)	C_{n1} (ppm)	R_{S1} KΩ	R_{S2} KΩ	α	Standard Uncertainty
2620	149.2632	223.8948	4.9051	4.3964	-0.2700	0.0549
			4.9377	4.4213	-0.2725	
			4.9316	4.4029	-0.2797	
			5.5506	4.4431	-0.5489	
			4.9255	4.4029	-0.2766	
832			2.3608	1.8729	-0.5709	0.0989
			2.4712	2.0407	-0.4720	
			2.5118	1.9930	-0.5705	
			3.0099	1.9815	-1.0311	
			2.5118	1.9930	-0.5705	
2201			2.0054	1.9806	-0.0307	0.0060
			2.0780	2.0530	-0.0298	
			2.0561	2.0530	-0.0037	
			2.0939	2.0811	-0.0151	
			2.0623	2.0530	-0.0112	

Table 4.13 Standard uncertainty of α in case of acetone.

Sensor	C_{n1} (ppm)	C_{n1} (ppm)	R_{S1} KΩ	R_{S2} KΩ	α	Standard Uncertainty
2620	116.3698	174.5546	1.3217	0.9872	-0.7197	0.0183
			1.3560	1.0040	-0.7413	
			1.3307	0.9963	-0.7139	
			1.3258	1.0147	-0.6594	
			1.3405	1.0313	-0.6469	
832			3.1672	1.5597	-1.7470	0.0182
			3.5960	1.5631	-2.0548	
			3.5311	1.6858	-1.8235	
			3.3350	1.7759	-1.5542	
			3.2220	1.5978	-1.7297	
2201			4.6276	3.8650	-0.4441	0.0121
			4.7424	3.8860	-0.4912	
			4.7084	3.8913	-0.4701	
			4.6804	3.9208	-0.4368	
			4.6786	3.9398	-0.4239	

Table 4.14 Standard uncertainty of α in case of 2-Propanol.

Sensor	C_{n1} (ppm)	C_{n1} (ppm)	R_{S1} KΩ	R_{S2} KΩ	α	Standard Uncertainty
2620	111.7476	167.6215	1.7169	1.4207	-0.4669	0.0081
			1.7595	1.4304	-0.5107	
			1.7361	1.4233	-0.4899	
			1.7436	1.4258	-0.4962	
			1.7609	1.4567	-0.4676	
832			2.8422	2.1090	-0.7358	0.0425
			3.1408	2.1293	-0.9586	
			2.9980	2.1138	-0.8618	
			2.9425	2.1218	-0.8065	
			2.9638	2.2032	-0.7314	
2201			4.3784	3.9184	-0.2737	0.0138
			4.4823	3.9507	-0.3114	
			4.4347	3.9616	-0.2782	
			4.4163	3.9782	-0.2576	
			4.4482	4.0571	-0.2270	

Apart from these parameters, output response may deviate due to some external sources, such as ageing of the sensors, sensor poisoning, and environmental variation etc. known as

sensor drift. It can be compensated by using other algorithms. Although, EUC cannot be eliminated completely, its minimum level reflects the goodness of the system.

The uncertainties in measurement of V_{RL} due to direct-interface parameters of (4.23) were calculated by using (4.13) as shown in Table 4.15. Table 4.15 shows that the sensor responses (V_{RL}) measured for four gases are 0.9114 V, 0.4372 V, 1.3116 V and 1.0746 V for G1, G2, G3 and G4 respectively. The best uncertainty for TGS 2620 demonstrated in case of methanol is 78.8955 µV while poorest uncertainty is shown for acetic acid as 0.78 mV. The uncertainty in measurement of V_{RL} is contributed by all parameters, however R_L contributes least uncertainty while α contributes highest uncertainty. Similarly for other two sensor the highest and the least uncertainty contribution is from α and R_L.

On the other hand the uncertainty of measurement of sensor response (V_{RL}) is shown in Table 4.16 which shows that poorest uncertainty is in case of TGS 2620 and TGS 2201 is 1.2 mV while the best uncertainty in case of TGS 832 is 1.0 mV. The poorest uncertainty of 1.2 mV in case of TGS 2620 and TGS 2201 is highly contributed by C (0.92 and 1.1 mV) and least contributed by R_2 (0.88 µV and 1.17 µV).

Again the best uncertainty in V_{RL} is shown in case of TGS 832 (1.0 mV) which is again due to C (0.88 µV). Based on the uncertainty budget shown in Table 4.15 and 4.16 an uncertainty rank for measurement of V_{RL} can be assigned to each parameter as shown in Table 4.17.

Table 4.17 illustrates the rank wise uncertainty contribution of the sensor circuit parameter and direct-interface parameter while measuring V_{RL}. It is observed that the maximum uncertainty of the sensor circuit is contributed by α, while in case of direct-interface circuit the maximum contributor of uncertainty is from capacitors (C). Thus we can conclude that to improve the precision of measurement of V_{RL} a more precise value of C is necessary since it contributes the highest uncertainty among all the parameters in Table 4.17. For sensor circuit, the highest uncertainty is contributed by α (Rank-1) which interprets that the gas samples used in the experiments may have variation in concentration and purity. Moreover factors like reactive impurity [8] and variation in measurement of volume of

liquid etc. affects the gas concentration as well as the conductivity of the gas sensors, thereby resulting in uncertainty contributed by α .

Table 4.15 Uncertainty estimation for sensor parameters with four tested gases.

Parameter	Gas	Measured Value			Sensitivity			Uncertainty (V) $\times 10^{-5}$ (Standard Uncertainty)		
		2620	832	2201	2620	832	2201	2620	832	2201
V_c(V)	G1	5.0573			0.9999	1	0.9998	0.0265	2.8900	2.8894
								(0.0289×10^{-3})		
	G2				0.9994	0.9999	0.9982	2.8884	2.8896	2.8847
								(0.0289×10^{-3})		
	G3				0.9999	1	0.9997	2.8898	2.8900	2.8892
								(0.0289×10^{-3})		
	G4				0.9999	0.9999	0.9994	2.8898	2.8898	2.8883
								(0.0289×10^{-3})		
$R_L(\Omega)$	G1	461.83	462.9	465.7	9.19×10^{-7}	1.43×10^{-7}	2.37×10^{-6}	0.0265	0.0041 (0.0289)	0.0685
	G2				6.13×10^{-6}	1.36×10^{-6}	1.99×10^{-5}	0.1771	0.0393 (0.0289)	0.5756
	G3				7.72×10^{-7}	5.80×10^{-9}	2.81×10^{-6}	0.0223	0.0001 (0.0289)	0.0814
	G4				6.36×10^{-7}	7.34×10^{-7}	6.29×10^{-6}	0.0184	0.0212 (0.0289)	0.1819
C_n(ppm)	G1		211.214		1.22×10^{-6}	3.00×10^{-7}	2.23×10^{-6}	2.230	0.5481 (18.270)	4.078
	G2		149.263		5.12×10^{-6}	2.40×10^{-6}	1.90×10^{-6}	6.612	3.104 (12.911)	2.463
	G3		116.369		2.20×10^{-6}	4.03×10^{-8}	5.00×10^{-6}	2.222	0.0406 (10.066)	5.041
	G4		111.747		2.01×10^{-6}	2.23×10^{-6}	7.27×10^{-6}	1.951	2.163 (9.666)	7.035
α	G1	0.6071	0.9531	0.4269	0.0023	3.55×10^{-4}	0.0059	7.001 (0.0308)	2.551 (0.0717)	10.05 (0.0170)
	G2	0.27	0.57	0.0307	0.0142	0.0032	0.0464	77.80 (0.0549)	31.17 (0.0989)	27.86 (0.0060)
	G3	0.7197	1.7470	0.4441	0.0017	1.27×10^{-5}	0.0062	3.107 (0.0183)	0.0232 (0.0182)	7.554 (0.0121)
	G4	0.7669	0.7358	0.2773	0.0014	0.0016	0.0138	1.123 (0.0081)	6.811 (0.0425)	19.08 (0.0138)
V_{RL}(V)	G1	0.9114	1.0103	0.6967	-	-	-	7.895	3.894 (-)	11.22
	G2	0.4372	0.0918	0.1145				78.14	31.46 (-)	28.13
	G3	1.3116	0.6461	0.4610				4.789	2.890 (-)	9.532
	G4	1.0746	0.7095	0.4847				3.663	7.709 (-)	20.54

Table 4.16 Uncertainty estimation for DIC local parameters for three gas sensors (TGS 2620, TGS 832, TGS 2201).

Parameter	Estimated/ Measured value			Sensitivity			Uncertainty (V) $\times 10^{-5}$ (Standard uncertainty)		
	2620	832	2201	2620	832	2201	2620	832	2201
V_{IH} (V)		1.962		1.2505	1.2407	1.2897	3.6139	3.5856	3.7272
							(0.0289×10^{-3})		
$R_1(\Omega)$	3197	3205	3211	2.3429×10^{-4}	2.2378×10^{-4}	2.7350×10^{-4}	6.7709	6.4671	7.9043
								(0.289)	
$R_2(\Omega)$	9861	9951	9961	3.0566×10^{-6}	2.7685×10^{-6}	4.0766×10^{-6}	0.0883	0.080	0.1178
								(0.289)	
V_{DD} (V)		4.65		0.2505	0.2407	0.2897	0.7239	0.695	0.8371
							(0.0289×10^{-3})		
C(μF)	2.255	2.256	2.116	$3.1897\times10^{+5}$	$3.0570\times10^{+5}$	$3.9585\times10^{+5}$	92.13	88.34	110
								(2.89)	
N	768	790	717	0.0011	0.0011	0.0012	73.66	48.15	38.896
							(0.6609)	(0.435)	(0.3232)
t_{loop} (μs)		2.601		$2.7631\times10^{+5}$	$2.6508\times10^{+5}$	$3.2195\times10^{+5}$	26.24	25.18	30.585
							(0.95×10^{-3})		
V_{RL} (V)	1.10	1.16	1.05		-		120	100	120
								(-)	

Table 4.17 Rank of parameters in EUC in V_{RL} measurement.

Rank	Sensor	Direct Interface circuit
	For all gases	For all sensors
1	α	C
2	C_n	N
3	V_C	t_{loop}
4	R_L	R_1
5	-	V_{IH}
6	-	V_{DD}
7	-	R_2

4.7. Conclusion

This study has addressed the nonlinearity problem prevalent in analog voltage measurement of a single sensor based DIC by proposing an optimized error compensation technique. The proposed technique has been compared with the ideal ADC and promising results were achieved. An online comparison of the proposed system with the

uncompensated DIC and ADC based system established the viability of the system. Moreover a multisensory measurement system is designed and developed using the proposed technique which is incorporated in an E-Nose setup. Experimental findings indicate that the proposed multisensory measurement system approximates the ADC based system. Further a comparative study on offline and online gas discrimination using the measured responses from the proposed system and an ADC based system reveals similar results. The technique reported here is not restricted to this particular application only, but it can be tested also for various practical multisensory systems. Further, this chapter addressed a protocol to measure uncertainties in DIC based multi-sensor framework. We have estimated the extent up to which the individual input parameter will cause variation in the output responses of the sensors under controlled condition. This gives us an insight about the overall deviation that may occur in the responses from which we can interpret the interval in which the output remains. Further it indicates that the measured sensors responses reliably represent its true value. Since in our estimation the uncertainties are very low compared to the output we believe that the quality of our E-Nose system is accurate and reliable. Moreover it should be kept in mind that while designing an E-Nose system utmost care should be taken to minimize and if possible eliminate the uncertainty sources. Although, in practical situations some of the uncertainty sources cannot be eliminated, the deviation caused by those uncertainty sources must be considered during any interpretation from the measured values for effective output representation.

References

[1]. Adams, T. M. G104-A2LA Guide for estimation of measurement uncertainty in testing. *American Association of Laboratory Accreditation Manual*, 10-18, 2002.

[2]. Bell, S. A beginner's guide to uncertainty of measurement. *Measurement good practice guide*, *11*, 1, 1999.

[3]. Bengtsson, L. Direct analog-to-microcontroller interfacing. *Sensors and Actuators A: Physical*, 179:105-113, 2012.

[4]. Bierl, L. Precise measurements with the MSP430. *Report Texas Instruments*, 1996.

[5]. Chen, Q. Zhao, J. Vittayapadung, S. Identification of green tea grade level using electronic tongue and pattern recognition, *Food Research International*, 41(5):500-504, 2008.

[6]. Cox, D. Implementing ohmmeter/temperature sensor. *Microchip Technology, Chandler, AZ, Appl. Note AN512*, 1997.

[7]. Custodio, A., Pallàs-Areny, R., and Bragós, R. Error analysis and reduction for a simple sensor-microcontroller interface. *IEEE Transactions on Instrumentation and Measurement*, 50(6):1644-1647, 2001.

[8]. Deshmukh, B. K., and Coetzee, J. F. Characterization of reactive impurities in methanol, ethanol, and 2-propanol by monitoring the activities of added ionic probes with ion selective electrodes. *Analytical Chemistry*, 56(13):2373-2378, 1984.

[9]. Dutta, L., Hazarika, A., and Bhuyan, M. Microcontroller based e-nose for gas classification without using ADC. *Sens. Transducers*, 202(7):38-45, 2016.

[10]. Dutta, L., Talukdar, C., Hazarika, A., and Bhuyan, M. A Novel Low-Cost Hand-Held Tea Flavor Estimation System. *IEEE Transactions on Industrial Electronics*, 65(6):4983-4990, 2018.

[11]. Gaitán-Pitre, J. E., Gasulla, M., and Pallas-Areny, R. Analysis of a direct interface circuit for capacitive sensors. *IEEE Transactions on Instrumentation and Measurement*, 58(9):2931-2937, 2009.

[12]. Gavin, H. The Levenberg-Marquardt method for nonlinear least squares curve-fitting problems. *Department of Civil and Environmental Engineering, Duke University*, 1-15, 2011.

[13]. Haghighat, M., Abdel-Mottaleb, M., and Alhalabi, W. Discriminant correlation analysis: Real-time feature level fusion for multimodal biometric recognition. *IEEE Transactions on Information Forensics and Security*, 11(9):1984-1996, 2016.

[14]. Han, J., Pei, J., and Kamber, M. *Data mining: concepts and techniques*. Elsevier, 2011.

[15]. Jordana, J., and Pallas-Areny, R. A simple, efficient interface circuit for piezoresistive pressure sensors. *Sensors and Actuators A: Physical*, 127(1):69-73, 2006.

[16]. Kokolanski, Z., Jordana, J., Gasulla, M., Dimcev, V., and Reverter, F. Direct inductive sensor-to-microcontroller interface circuit. *Sensors and Actuators A: Physical*, 224:185-191, 2015.

[17]. López-Lapeña, O., Serrano-Finetti, E., and Casas, O. Low-power direct resistive sensor-to-microcontroller interfaces. *IEEE Transactions on Instrumentation and Measurement*, 65(1):222-230, 2016.

[18]. Peter, D., Baker, B. C., Butler, D., and Darmawaskita, H. Make a Delta-Sigma Converter Using a Microcontroller's Analog Comparator Module. *Microchip Technology Inc., Chandler, Arizona*, 1998.

[19]. Reverter, F., Gasulla, M., and Pallàs-Areny, R. A low-cost microcontroller interface for low-value capacitive sensors. In *Instrumentation and Measurement Technology Conference, 2004. IMTC 04. Proceedings of the 21st IEEE* (Vol. 3, pp. 1771-1775). IEEE, 2004.

[20]. Reverter, F., Jordana, J., Gasulla, M., and Pallàs-Areny, R. Accuracy and resolution of direct resistive sensor-to-microcontroller interfaces. *Sensors and Actuators A: Physical*, 121(1):78-87, 2005.

[21]. Reverter, F., Gasulla, M., and Pallàs-Areny, R. Analysis of power-supply interference effects on direct sensor-to-microcontroller interfaces. *IEEE Transactions on Instrumentation and Measurement*, 56(1):171-177, 2007.

[22]. Reverter, F., and Casas, O. Direct interface circuit for capacitive humidity sensors. *Sensors and Actuators A: Physical*, 143(2):315-322, 2008.

[23]. Reverter, F., and Casas, O. Interfacing differential resistive sensors to microcontrollers: A direct approach. *IEEE Transactions on Instrumentation and Measurement*, 58(10):3405-3410, 2009.

[24]. Reverter, F., and Casas, Ò. A microcontroller-based interface circuit for lossy capacitive sensors. *Measurement Science and Technology*, 21(6):065203, 2010.

[25]. Reverter, F., and Casas, Ò. Interfacing differential capacitive sensors to microcontrollers: A direct approach. *IEEE Transactions on Instrumentation and Measurement*, 59(10):2763-2769, 2010.

[26]. Richey, R. (1997). Resistance and capacitance meter using a PIC16C622. *AN611, Chandler (AZ), Microchip Technology*.

[27]. Sifuentes, E., Casas, O., Reverter, F., and Pallas-Areny, R. Direct interface circuit to linearise resistive sensor bridges. *Sensors and Actuators A: physical*, 147(1):210-215, 2008.

[28]. Soldera, J. D. B., Espindola, M., and Olmos, A. Implementing a 10-bit Sigma-Delta Analog-to-Digital Converter Using the HC9S08Rx MCU Family Analog Comparator. *Freescale Semiconductor*, 1-22, 2005.

[29]. www.wolframalpha.com/

[30]. Yamazoe, N., and Shimanoe, K. Theory of power laws for semiconductor gas sensors. *Sensors and Actuators B: Chemical*, 128(2):566-573, 2008.

[31]. Zhang, L., Tian, F., Nie, H., Dang, L., Li, G., Ye, Q., and Kadri, C. Classification of multiple indoor air contaminants by an electronic nose and a hybrid support vector machine. *Sensors and Actuators B: Chemical*, 174:114-125, 2012.

[32]. Zhang, L., and Zhang, D. Domain adaptation extreme learning machines for drift compensation in E-nose systems. *IEEE Transactions on instrumentation and measurement*, 64(7):1790-1801, 2015.

[33]. Zhang, L., and Zhang, D. Efficient solutions for discreteness, drift, and disturbance (3D) in electronic olfaction. *IEEE Transactions on Systems, Man, and Cybernetics: Systems (in press)*, 2016.

[34]. Zhang, L., and Zhang, D. Evolutionary cost-sensitive extreme learning machine. *IEEE transactions on neural networks and learning systems*, 28(12):3045-3060, 2017.